Brain Structure and Function 226 (2021): 845 – 859

DOI: https://doi.org/10.1007/s00429-020-02213-4

PUBLISHED APRIL 2021
BRAIN STRUCTURE & FUNCTION, 226, 3, 845-859
https://doi.org/10.1007/s00429-020-02213-4

Brain resilience across the general cognitive ability distribution:

Evidence from structural connectivity

Javier Santonja[1], Kenia Martínez[1], Francisco J. Román[1], Sergio Escorial[2]

Mª Ángeles Quiroga[2], Juan Álvarez-Linera[3], Yasser Iturria-Medina[4]

Emiliano Santarnecchi[5], Roberto Colom[1]*

(1) Universidad Autónoma de Madrid
(2) Universidad Complutense de Madrid
(3) Hospital Ruber Internacional
(4) Montreal Neurological Institute
(5) Harvard Medical School

(*) Corresponding author
Facultad de Psicología
Univesidad Autónoma de Madrid
28049 Madrid (Spain)
Email: roberto.colom@uam.es

Acknowledgements

The study reported here was supported by research project 'PSI2017-82218-P' funded by 'Ministerio de Economía, Industria y Competitividad' (Spain). We thank MENSA-Spain for supporting the recruitment of high cognitive ability volunteers that participated in the present research. We thank Human Connectome Project (HCP) for providing access to their database and for addressing our questions regarding sample characteristics. We also thank the University of Pennsylvania for providing access to their computerized neuropsychological battery.

Abstract and Keywords

Resting state functional connectivity research has shown that general cognitive ability (GCA) is associated with brain resilience to targeted and random attacks (TAs and RAs). However, it remains to be seen if the finding generalizes to structural connectivity. Furthermore, individuals showing performance levels at the very high area of the GCA distribution have not yet been analyzed in this regard. Here we study the relation between TAs and RAs to structural brain networks and GCA. Structural and diffusion-weighted MRI brain images were collected from 189 participants: 60 high cognitive ability (HCA) and 129 average cognitive ability (ACA) individuals. All participants completed a standardized fluid reasoning ability test and the results revealed an average HCA-ACA difference equivalent to 33 IQ points. Automated parcellation of cortical and subcortical nodes was combined with tractography to achieve an 82x82 connectivity matrix for each subject. Graph metrics were derived from the structural connectivity matrices. A simulation approach was used to evaluate the effects of recursively removing nodes according to their network centrality (TAs) versus eliminating nodes at random (RAs). HCA individuals showed greater network integrity at baseline and prior to network collapse than ACA individuals. These effects were more evident for TAs than RAs. The networks of HCA individuals were less degraded by the removal of nodes corresponding to more complex information processing stages of the PFIT network, and from removing nodes with larger empirically observed centrality values. Analyzed network features suggest quantitative instead of qualitative differences at different levels of the cognitive ability distribution.

Keywords. Cognition, Brain Connectomics, Network Integrity, Brain Resilience

1. INTRODUCTION

Individual differences in general cognitive ability (GCA), as assessed by standardized tests, are correlated with structural and functional brain features (A. K. Barbey et al., 2012; Colom et al., 2013; Ebisch et al., 2012; Gignac & Bates, 2017; Gläscher et al., 2009, 2010; Karama et al., 2011; Román et al., 2014; Vakhtin, Ryman, Flores, & Jung, 2014). However, the meta-analysis by Basten, Hilger, & Fiebach, (2015) highlighted that these two brain features show non-overlapping correlates with cognitive ability differences. Therefore, structural and functional support of cognitive abilities might not be found within the same regions and networks. Simply assuming that findings derived from structural and functional neuroimaging research will overlap is not warranted. Euler (2018) suggests that this dissociation between structural and functional correlates of cognitive ability represents "the deep and intriguing possibility that cognitive ability might be structured somewhat differently in different individuals" (p. 101).

Indeed, there are substantial differences in published findings regarding the most likely correlates at the brain level of assessed cognitive ability differences (Colom, 2014; Euler, 2018). Neuroimaging approaches based on completed tasks and on individual differences may reveal quite different evidence. The first approach quantifies the mean task evoked activation in a predefined group of individuals, neglecting the probable relationship between individual differences in brain activation and variations in cognitive performance. The second approach focuses on the associations between individual differences at the cognitive and brain levels. Moreover, the use of different neuroimaging protocols can lead to remarkable discrepancies (Martínez et al., 2015). The considered brain features, the nature of the analyzed sample of individuals, the way intelligence is

measured, or the covariates of interest (sex, age, etc.) are among the main factors contributing to these discrepancies in hardly identifiable ways (Colom, Karama, Jung, & Haier, 2010; Colom & Thompson, 2011; Escorial et al., 2015; Martínez & Colom, 2021).

For overcoming this situation, lesion approaches might shed some light. Vaidya, Pujara, Petrides, Murray, & Fellows (2019) have argued that brain lesion studies "provide unique, vital insights into brain function that cannot be achieved via temporary inactivation methods or correlational studies of brain activity" (p. 656). Large-scale studies analyzing the impact of focal and chronic brain lesions using a voxel-based lesion-symptom mapping (VBLSM) approach have supported the relevance of frontal-parietal networks for intelligence or GCA (A. Barbey, Colom, Paul, & Grafman, 2014; A. K. Barbey et al., 2012; Gläscher et al., 2009, 2010). Importantly, VBLSM identifies brain areas that might play a 'causal' role in cognitive performance differences by comparing individuals with and without a lesion at the voxel level.

Relatedly, using a simulation approach for analyzing resting state fMRI data of 102 healthy individuals, (Santarnecchi, Rossi, & Rossi, 2015) have shown that individual differences in GCA are correlated with brain resilience. They applied a network framework in which brain resilience was quantified using two approaches based on targeted and random attacks (TAs and RAs) to network integrity. TAs did test the relevance of the considered nodes/regions regarding network stability, whereas RAs did test this stability by checking system failure. Initial network integrity indices were computed before applying progressive node removal and robustness drops were systematically computed by assessing integration and segregation network indices. The correlation between resilience to TAs and GCA was $r = 0.65$, whereas the value for RAs

was $r = 0.45$. Both values represent a very large effect size (Funder & Ozer, 2019). These findings were interpreted as supporting the perspective that individuals with higher GCA do have a greater distributed information processing capacity: "this may give reason of the better capacity to keep the network working properly on the ground of a less-centralized system, where different operations may be successfully executed along different paths" (p. 305). Nevertheless, there were a set of important areas with regard to network connectivity resilience within the parietal, frontal and temporal brain lobes, especially the pars opercularis of the inferior frontal gyrus, the inferior parietal lobe, and the middle frontal gyrus.

The present study was designed for testing if this functional evidence generalizes to structural connectivity data. In addition, we will test if individuals with very high levels of general cognitive ability (HCA) –achieving test scores within the top 2% of the general population—do show greater brain structural resilience to both TAs and RAs than average cognitive ability (ACA) individuals. The default hypothesis is that the greater distributed processing capacity that may characterize HCA individuals will support their greater resilience to attacks directed to their structural connectome. We also predict that the brain network defining the parietal-frontal integration theory of intelligence (P-FIT) (Jung & Haier, 2007) will be key for predicting brain resilience variations at the individual level with increased node removal based on both TAs and RAs.

With these goals in mind, the current study analyzes brain images of one hundred and eighty-nine individuals scanned using the HCP (Human Connectome Project) multi-shell diffusion tensor imaging protocol. The data was submitted to image analyses for identifying individual connectomes. Afterwards, integrity indices (global and local

efficiency) were quantified after increased node removal (TAs and RAs). First, the method by which network integrity is progressively degraded with increased numbers of attacks was computed. The prediction here is that HCA individuals will show greater brain resilience across the increased numbers of attacks, meaning that network integrity will be higher and preserved longer than in ACA individuals. Secondly, the relationship between fluid reasoning ability scores and the change in the considered network integrity indices comparing initial values and those obtained just before the network becomes disconnected was studied. The prediction here is that the higher the cognitive ability score, the greater the network integrity computed when this fatal point is achieved. Finally, we looked for the most relevant (central) nodes/regions in HCA and ACA individuals with respect to both their connectivity and their relevance for triggering a network breakdown using a theory-driven and a data-driven approach.

2. METHODS

2.1. Participants

Sixty high cognitive ability (HCA) individuals were recruited from MENSA-Spain. There are more than 140,000 members across 100 countries in MENSA International from whom around 1750 live in Spain. The association includes high IQ individuals and members must pass a complex test designed for screening the top 2% of the general population (98^{th} percentile on a standard test of intelligence). Furthermore, one hundred and twenty average cognitive ability (ACA) individuals were selected from the Human Connectome Project (HCP) public database (http://www.humanconnectomeproject.org) to represent a range of cognitive ability within the normal range. Finally, nine controls of average cognitive ability were scanned in the same site as the HCA individuals using

exactly the same MRI acquisition parameters. All participants completed the same general reasoning ability computerized test (see below for details).

Two HCA participants were discarded because they lacked appropriate DTI data. Therefore, the final sample included 58 HCA and 129 ACA individuals (grand total = 187). HCA were older (mean age = 34.2; SD = 6.9) than ACA individuals (mean age = 29.9, SD = 3.5) [t (185) = 4.5; d = 0.89; p = .000] and they also showed (as expected) much higher values on the fluid reasoning test [t (185) = -19.2; d = 2.22; p = .000] (Figure 1). The sex distribution for HCA (60% men) and ACA (52% men) individuals were roughly equivalent ($\chi^2(1)$=1.14; p=.29).

FIGURE 1 AROUND HERE

2.2. Fluid reasoning test

All participants completed the Penn Matrix Reasoning Test (PMAT-24). This multiple-choice computerized test is included in the Penn Computerized Neurocognitive Battery (Dubois, Galdi, Paul, & Adolphs, 2018; Moore, Reise, Gur, Hakonarson, & Gur, 2015) and comprises problems based on spatial and numerical relationships. The problems are ordered by increased cognitive complexity and they display patterns made up of 3x3, 2x2, or 1x5 arrangements of squares. One of these squares is missing. Examinees must select the one, among five alternatives, that best fits the missing square. The items are designed after the conceptual framework considered by the Raven's Progressive Matrices Test and the Matrix Reasoning subscale from the WAIS-III.

2.3. MRI acquisition

Neuroimaging data of sixty HCA individuals and nine ACA individuals were acquired in a 3T Siemens Magnetom Prisma at Ruber Internacional Hospital (Madrid). Images of 120 ACA individuals were recovered from the Human Connectome Project (HCP) public database. The MRI Scans of interest for the present study contained a structural session (T1-weighted image and T2-weighted image) and a Multi-Shell Diffusion Tensor Image (DTI) session. The acquisition parameters for the Madrid individuals were: T1weighted images: 0.8 mm isotropic voxel sixe, a 220 Hz/Px bandwidth, TR = 2400 ms. and TE = 2.22 ms; T2 weighted images: 0.8 mm isotropic voxel, a 744 Hz/Px bandwith, TR = 3200 ms. and TE = 563 ms; Diffusion weighted images: 98 directions, 1.5 mm isotropic voxel, 1700 Hz/Px bandwith, TR = 3230 ms., TE of 89.20 ms, multiband factor of 4, echo spacing = 0.69 and b-values of 0 and 3000 s/mm^2. The acquisition parameters for the HCP individuals were: T1weighted images: 0.7 mm isotropic voxel, 210 Hz/Px bandwidth, TR = 2400 ms. and TE = 2.14 ms; T2 weighted images: 0.7 mm isotropic voxel, 744 Hz/Px bandwidth, TR = 3200 ms. and a TE = 565 ms; Diffusion weighted images: 97 directions, 1.25 isotropic voxel, 1488 Hz/Px bandwidth, TR = 5520 ms., a TE = 89.5 ms., a multiband factor of 3, echo spacing = 0.78 ms., and b-values of 1000, 2000 and 3000 s/mm^2. Therefore, the acquisition parameters were almost identical for the HCA and ACA individuals. Technicians from the Siemens company carefully checked their equivalence.

2.4. Image processing

Structural images were processed with the Freesurfer software suite (version 6.0) to segment the T1-weighted images into 82 regions, comprised of 68 cortical regions and 14 subcortical regions (Desikan et al., 2006; Fischl et al., 2004). Furthermore, T1-weighted images were also segmented into a 5-tissue type parcellation using FSL (https://fsl.fmrib.ox.ac.uk/).

DWI images were pre-processed using the MRTrix software (http://www.mrtrix.org/). The steps included in the DWI images pre-processing pipeline comprise denoising, bias correction, and distortion correction. The latter included correcting the susceptibility induced distortions using FSL's tool *topup*, and later correcting the eddy current induced resonance fields using FSL's tool *eddycorrect*, taking the *b0* volume as the reference image in both cases.

For building the DWI connectome, anatomically-constrained probabilistic tractography was applied to the pre-processed DWI images using MRTrix software suite. The five Tissue Type T1-segmented image was used as anatomical reference after being registered to the *b0* volume of the DWI data. After estimating the white matter response functions and obtaining the fiber orientation distribution for each tissue type, an initial tractogram of 10 million streamlines was generated, with restrictive measures that included cropping streamlines at the grey/white matter interface, allowing a maximum length of 250 millimeters per streamline and a maximum fiber orientation distribution of 0.06. This tractogram was filtered down to a 1 million streamlines tractogram using MRTrix "Spherical-deconvolution Informed Filtering of Tractograms" (SIFT) algorithm (Smith, Tournier, Calamante, & Connelly, 2013).

The DWI connectome matrix was created by writing the value at the position (X,Y) of the matrix as the number of streamlines that connect region X with region Y in the aforementioned Freesurfer parcellation. This resulted in an 82x82 connectivity matrix for each individual. Figure 2a summarizes these processing steps.

FIGURE 2 AROUND HERE

The network connectome that was calculated for each individual in this study comes directly from the output of the MRTrix software (https://www.mrtrix.org). Specifically, the function "tck2connectome" makes use of the 82 regions of the Desikan-Kelliany Atlas to create an 82x82 matrix in which the edge weights are the streamlines (or tracks) connecting these regions. A streamline is a mathematical line that connects two regions through the brain's white matter. This streamline is generated using information from the Diffusion-Weighted images regarding how the diffusion of water molecules behaves within the white matter, and how this diffusion is affected by the constrains given by the anatomical fibers. Therefore, streamlines tend to follow the same direction as the white matter physiological fibers. MRTrix is a probabilistic streamline generation approach, which means that the endpoints of the streamlines are not pinpointed from the streamlines' seeds. Instead, the path of the streamline is guided, step by step, on a probability distribution of the diffusion of a water molecule in a specific direction. According to this, it is possible that two streamlines that start at the same point end up at a different region. In our research study, the number of streamlines connecting two regions reflect the likelihood of those regions having a more robust connection. This is so because the seed points and the end points of the streamlines were the same (1 million streamlines were calculated for each individual). Therefore, a higher number of streamlines relates to a larger level of network integrity among regions.

2.5. Network lesioning

To test network resilience against attacks, two types of network lesioning procedures were implemented, based on the targeted or random removal of nodes from the connectivity matrix (Figure 2 b to d). All the graph properties have been calculated using MATLAB functions included in the Bioinformatics toolbox and the built-in graph theory libraries.

In order to explain the procedures, it must be noted that (N) is the set of nodes in the network, (n) is the number of nodes, (k) is a specific node, (L) is the set of all links in the network, (l) is the number of links, (i,j) is the link between nodes i and j, and (a_{ij}) is a binary connection status between i and j (1 when the link exists, 0 otherwise).

2.5.1. Targeted attacks (TAs)

Regarding targeted attacks (TAs) individual betweenness centrality indices were calculated for serving as criteria in the order for removing nodes. This specific order is related to the role the node plays in the properties of interest of the network, namely, the importance of the node for distributed information processing. Previous studies on brain robustness suggest "centrality" measures as providing the best robustness estimation (Alstott, Breakspear, Hagmann, Cammoun, & Sporns, 2009).

The betweenness centrality (Bc) of a node k refers to the fraction of shortest paths between two nodes in N that go through node k with respect to the total number of shortest paths. In this case, Bc for the node i is defined as:

$$\mathrm{Bc_i} = \frac{1}{(\mathrm{n}-1)(\mathrm{n}-2)} \sum_{\substack{\mathrm{h,j \in N} \\ \mathrm{h \neq j, h \neq i, j \neq i}}} \frac{\rho_{\mathrm{hj}}(\mathrm{i})}{\mathrm{p_{hj}}}$$

where p_{hj} is the number of shortest paths between h and j, and $\rho_{hj}(i)$ is the number of shortest paths between h and j that pass through i

The lesioning process regarding TAs involved (1) computing the centrality value for all nodes at the individual level (Figure 2 b), (2) sorting the importance of these nodes according to their centrality values for each individual (Figure 2 c), (3) removing the node with the highest centrality value, and (4) recursively applying the previous steps until all nodes are removed (Figure 2 d). Therefore, centrality values were computed separately for each of the analyzed 187 individuals, which, among other things, allows knowing if these nodes are ordered in the same way across individuals. Furthermore, it is also possible to check (a) if their connectome breaks-down as a consequence of removing the same number of nodes, and (b) if integrity indices across increasingly numbers of attacks change at different rates for different individuals.

2.5.2. Random attacks (RAs)

With respect to the randomized attacks (RAs) the removal of nodes in a random order simulates the occurrence of a system failure (Santarnecchi et al., 2015). The fact that a network might be resilient against RAs discloses the robustness and integrity of the global processing network.

First, a list of randomly ordered regions is generated for each individual. The nodes representing these regions were removed following the order on this random list. To ensure the reliability of the RAs procedure, the whole methodology was applied 100 times and the integrity estimates were averaged (Figure 2 d).

2.6. Network integrity measures

To study the integrity and resilience of the networks against TAs and RAs, network integrity measures were computed before node removal and after progressive node removal. Network integrity values were systematically checked with increased node removal. Nevertheless, one further index was calculated to know at which point the network becomes disconnected: the number of node depletions (ND) before network collapse. Because the effect of removing a given node is very damaging to the whole network, this index will only be used to calculate the average of the other indices leaving out the values obtained from a disconnected network.

To understand how network lesioning changes integration and segregation of information processing, network integrity measures were divided on distributed processing and local processing. For the distributed processing analyses Global Efficiency (GE) was calculated as the average across all nodes of all the shortest paths in the network that go through each node (Sporns & Zwi, 2004). Therefore, a higher *GE* value would represent better overall information processing throughout the brain.

$$GE = \frac{1}{n}\sum_{i\in N}\frac{\sum_{j\in N, j\neq i} d_{ij}^{-1}}{n-1}$$

where d_{ij} represents the distance matrix whose values represent the shortest path length between all pairs within the set nodes N (Santarnecchi, Galli, Polizzotto, Rossi, & Rossi, 2014).

For quantifying local processing, the Local Efficiency Index (LE) was calculated. LE represents the average network efficiency across all the neighboring subgraphs of the network. The neighboring subgraph of a node corresponds to the subgraph formed by the neighbors of this node, but not by itself. Hence, a higher value of LE is indicative of the information processing at small local levels in the brain.

$$LE = \frac{1}{n}\sum_{i \in N} Le_i = \frac{1}{n}\sum_{i \in N} \frac{\sum j, h \in N, j \neq a_{ij}a_{ih}[d_{jh}(N_i)]^{-1}}{k_i(k_i - 1)}$$

where LE_i is the local efficiency of node i, and $d_{jh}(N_i)$ is the length of the shortest path between j and h, that contains only neighbors of i.

2.7. Statistical analyses

First, the distribution of ND (number of depletions) before network collapse was considered for verifying potential differences between HCA and ACA individuals regarding network disintegration after TAs and RAs. *t* tests were computed for analyzing differences in ND and PMAT scores in HCA and ACA individuals. After addressing this goal, individual values of network integrity indices (GE and LE) were considered at different stages of network disintegration, always before network collapse at the individual level. For TAs, they were organized in five bands: after removing 0 (baseline), 10, 20, 30, and 40 nodes. Several 2 x 5 ANOVAs (group x nodes) were computed. 'Nodes' was a repeated measures factor with the values of GE and LE in the different bands (0, 10, 20, 30, and 40). This analysis allowed to study if HCA and ACA individuals were different in their network integrity before and after removing nodes. For RAs, two more values were added (after 50 and 55 nodes were removed) since most networks resist

for a longer time against RAs. The ANOVAs were computed with seven levels in the repeated-measures factor (0, 10, 20, 30, 40, 50, and 55 nodes).

Network collapse is defined as the moment in the sequence of node removals in which the network becomes disconnected. There are only two theoretical scenarios in which this occurs: either the total number of nodes in the network becomes zero, or the distance between any two nodes in the network becomes infinite (the network has two or more distinctly separated components). In this process, the moment right before any of these scenarios occurs has been measured after the Number of Depletions (ND) that it takes in each network to reach collapse.

Second, the change in every network integrity index was calculated as the difference between the value of the index just before the individual network collapses (at $ND - 1$ nodes removed) minus the initial value of the index when no perturbation had occurred (0 nodes removed). This was done for TAs and RAs. The change score computed for both individuals (HCA and ACA) was compared using *t* tests. In addition, change values were related to fluid reasoning scores (PMAT-24) using the Spearman rank-order correlation (r_s).

Finally, theory and data-driven approaches were applied for identifying the nodes with greater relevance for network integrity in HCA and ACA individuals. The first approach is based on the parieto-frontal integration theory of intelligence (P-FIT). The procedure requires deleting the relevant nodes within the four processing stages stipulated by the theory (Pineda-Pardo, Martínez, Román, & Colom, 2016): (1) processing of sensory information involves occipital and temporal regions, especially the fusiform gyrus and

Wernicke's area; (2) integration and abstraction of the sensory information is supported by the angular gyrus, the supramarginal gyrus, and the superior parietal lobe; (3) evaluation and hypothesis testing recruit frontal regions mainly; and (4) response selection involves the anterior cingulate. The nodes supporting each processing stage were removed, step by step, to evaluate how integrity values change for HCA and ACA individuals. For the data-driven approach, (a) the nodes showing the highest betweenness values were selected, (b) deleted, and (c) the integrity values after this node removal was computed. 2 x 2 ANOVAs (group x nodes) were computed for all P-FIT processing stages and for the data-driven approach regarding GE and LE values. Nodes was a repeated measures factor with two levels: network integrity at baseline and network integrity after removing nodes.

3. RESULTS

First, the ND required for network collapse was similar for HCA (mean ND-TAs = 38 nodes, SD = 11.7; mean ND-RAs = 51 nodes; SD = 17.0) and ACA (mean ND-TAs = 39 nodes; SD = 9.8; mean ND-RAs = 52 nodes, SD = 14.0) individuals. This applies both to TAs [$t(185)=.36$; $p=.72$] and RAs [$t(185)=.09$; $p=.93$] (Supplementary Figure 1). Due to the large harming capacity of node removal in relatively small-sized networks, this absence of differences between HCA and ACA individuals is good news because it is consistent with the conclusion that the identified connectomes can be properly compared without the menace of bias due to site registration or the use of MRTrix.

FIGURE 3 AROUND HERE

Figures 3 and 4 depict how network integrity values change, at the individual level, across increased numbers of TAs and RAs respectively. The left panels in both Figures show GE and LE values plotted against the state of network disintegration for each individual. Higher GE and LE represent greater overall and local information processing capacity respectively.

The results displayed in Figure 3 (left panel) suggest that HCA individuals (red dots) show greater integrity values (higher GE and LE) than ACA individuals (blue dots) at initial conditions (baseline) and just before network breakdown. The repeated measures ANOVA showed a significant nodes-by-group interaction effect for GE [$F(4,740) = 23.63$; $\eta^2_p = .11$; $p = .00000008$] and LE [$F(4,740) = 36.56$; $\eta^2_p = .17$; $p = .0000000$]. Post hoc comparisons revealed that, before any node removal, there was a significant mean difference between HCA and ACA individuals regarding GE [$F(1,185) = 9.0$; $\eta^2_p = .05$; $p = .003$] and LE [$F(1,185) = 7.44$; $\eta^2_p = .04$; $p = .007$]; and just before network breaks down this difference increased for both network integrity measures [GE: $F(1,185) = 24.19$; $\eta^2_p = .17$; $p = .000002$; LE: $F(1,185) = 44.71$; $\eta^2_p = .20$; $p = .0000000003$]. The values for GE and LE reflect better network integrity in HCA individuals before nodes removal (d values = 0.46 and 0.57, respectively) and, after the applied TAs, the difference increases (d values = 0.89 and 1.05, respectively).

FIGURE 4 AROUND HERE

As observed in the left panel of Figure 4, the evidence is less clear for RAs. HCA individuals showed greater integrity values (higher GE and LE) than ACA individuals at initial conditions (baseline) and just before network breakdown after RAs. The repeated

measures ANOVA showed a no significant nodes-by-group interaction effect for GE [$F(6,1110) = .72$; $\eta^2_p = .004$; $p = .48$] and LE [$F(6,1110) = .97$; $\eta^2_p = .005$; $p = .44$]. Nevertheless, a significant inter-subject effect was observed for both measures [GE: $F(1,185)=8.01$; $\eta^2_p = .04$; $p = .005$; LE: $F(1,185)=8.52$; $\eta^2_p = .04$; $p = .004$]. Therefore, the values for GE and LE reflect better network integrity in HCA individuals before nodes removal (baseline) and after RAs. These differences are stable across the number of progressive attacks until the network breaks down: *d* values at baseline were 0.46 for GE and 0.57 for LE, whereas *d* values at breakdown were 0.38 for GE and 0.52 for LE.

The right panels in Figure 3 (TAs) and Figure 4 (RAs) display individual change values in network integrity indices (Y-axis) plotted against PMAT-24 scores (X-axis). The changes in GE and LE were significantly higher in ACA individuals than in HCA for TAs [GE: $t(185)=4.59$; $p=.000008$; LE: $t(185)=5.21$; $p=.0000005$] but not for RAs [GE: $t(185)=.20$; $p=.83$; LE: $t(185)=.93$; $p=.42$]. The Spearman rank-order correlation values addressing the relationship between GE and the cognitive ability level were $r_s = -0.20$ ($p = .006$) for TAs and $r_s = 0.04$ ($p=.62$) for RAs. Regarding LE, the correlation values were $r_s = -0.25$ ($p = .001$) for TAs and $r_s = -0.07$ ($p=.33$) for RAs. Therefore, increased changes in network integrity after TAs was associated with lower cognitive performance.

Finally, we analyzed the relevance of some nodes within individual connectomes for explaining the observed differences in brain resilience using the theory-driven and data-driven approaches described above. First, we removed nodes included in the parieto-frontal integration theory of intelligence (P-FIT) according to the proposed processing stages. As shown in Figure 5 and Supplementary Table 1, network integrity values were smaller for ACA individuals when the nodes belonging to stage 2 were removed and, to

a lesser extent, for those nodes belonging to stage 4. The repeated measures ANOVA showed a significant nodes-by-group interaction effect for GE-Stage 2 [$F(1,185) = 15.06$; $\eta^2_p = .08$; $p = .0002$], LE-Stage 2 [$F(1,185) = 11.54$; $\eta^2_p = .06$; $p = .001$] and LE-Stage 4 [$F(1,185) = 6.70$; $\eta^2_p = .04$; $p = .01$]. Post hoc comparisons revealed that the initial significant mean differences between HCA and ACA individuals regarding network integrity measures, increased after removing nodes belonging to stage 2 and 4. These results suggest that HCA individuals were less affected by the removal of the nodes devoted to integration and response selection. Their connectomes seemed capable to overcome the imposed limitation presumably because of their higher distributed processing capacity. Findings for stages 1 and 3 are shown in the Supplemental Material.

FIGURE 5 AROUND HERE

Similar findings emerged from the data-driven approach (Figure 6), in which the most densely connected nodes were removed from the network. Figure 6a highlights the nodes with greatest betweenness (centrality) values for HCA and ACA individuals. For HCA individuals these nodes were (in descending order): right putamen, left putamen, left thalamus, right precuneus, left superior frontal, right superior frontal, left precuneus, right thalamus, left insula, right insula, left superior parietal, and right superior parietal (red and violet nodes in Figure 6a). For ACA individuals the nodes were: right putamen, right superior frontal, left superior frontal, left precuneus, left putamen, right precuneus, left isthmuscingulate, left insula, right insula, right isthmuscingulate, left superior parietal, and right thalamus (blue and violet nodes in Figure 6a). Therefore, 10 out of these 12 highly relevant (densely connected) nodes were common to HCA and ACA individuals:

bilateral putamen, bilateral precuneus, bilateral superior frontal, bilateral insula, left superior parietal, and right thalamus (violet nodes in Figure 6a).

FIGURE 6 AROUND HERE

After removing the most central nodes shared by HCA and ACA individuals (Figure 6, left panel), there was a visible decline in GE and LE (Figure 6, right panel) for ACA individuals, while the values were virtually unaltered in HCA individuals (Supplementary Table 1 includes the stats for the nodes removed-by-group interaction effect obtained from the repeated measures ANOVA).

4. DISCUSSION

4.1. Key findings

Here we have shown that high cognitive ability (HCA) individuals are more resilient to attacks, applied to their structural connectomes, than average cognitive ability (ACA) individuals. Their cognitive ability differences, assessed by a standardized test of fluid reasoning ability, was equivalent to 33 IQ points (d = 2.22), whereas their greatest difference in network integrity, assessed by global efficiency and local efficiency was d = 1.05. These differences reveal very high effect sizes (Funder & Ozer, 2019) but the former d value is much greater than the latter d value, which suggests that the observed differences separating HCA and ACA individuals at the brain level, using the analyzed structural data, can only partly account for their differences at the cognitive level. HCA's structural connectomes are more resilient, but their greater values must be seen as just one piece in the puzzle that scientific research is trying to solve regarding the biological

basis of human cognitive ability differences (A. K. Barbey, Karama, & Haier, 2021; Haier, 2017; Martínez & Colom, 2021; Sternberg, 2020).

Nevertheless, the general conclusion that the brains of HCA individuals are more resilient than the brains of ACA individuals at the structural level applies strongly to targeted attacks (TAs) and weakly to random attacks (RAs). TAs involved removing increased numbers of nodes in the network, beginning with the most central nodes, those showing highest betweenness values. The applied attacks stopped when the individual networks were disintegrated, and this happened almost at the same point in HCA and ACA individuals (approx. 40 nodes out for TAs and 55 for RAs of a maximum of 82). The evidence supports the conclusion that the difference in network integrity assessed before nodes removal becomes wider just before network disintegration. HCA individuals showed better network integrity from the outset, but their advantage widened with increased numbers of TAs (Figure 3). On the other hand, the nodes removed regarding RAs were (obviously) chosen at random for every individual. In this instance, the difference between HCA and ACA individuals was much weaker, albeit still present.

The big picture derived from the findings of the present investigation supports the view that HCA individuals keep their network integrity in the presence of applied attacks and this may happen because the enjoy a greater distributed processing capacity, as suggested by the functional neuroimaging study reported by (Santarnecchi et al., 2015): “the better capacity to keep the network working properly on the ground a less-centralized system, where different operations may be successfully executed along different paths.”

The latter conclusion was further supported by the findings derived from the theory-driven and data-driven node removal implemented here.

First, using the P-FIT model as framework, we defined a network including 12 nodes distributed across the four lobes, but clustered within four information processing stages: (1) processing of sensory information (temporal and occipital regions), (2) integration of information (parietal regions), (3) hypothesis testing (frontal regions), and (4) response selection (anterior cingulate). We have seen that removing P-FIT nodes included in stages 2 and 4 reduced network integrity in ACA individuals, but the effect over HCA individuals was much weaker. Interestingly, the P-FIT model stressed the relevance of the parietal areas for supporting higher cognitive ability and ACA findings are consistent with this assumption, whereas HCA findings are not. The resilient behavior of their networks against attacks applied to stage 2 nodes (precuneus, superior parietal, and supramarginal gyrus) might imply that HCA individuals can overcome network instability using alternative connections which, again, may support the greater distributed processing capacity of their networks. The fact that the relevance of the P-FIT network may change for different individuals was acknowledged by the authors (Haier, 2017; Jung & Haier, 2007) and the findings observed here for ACA and HCA individuals suggest that this might be indeed the case.

Secondly, closely related findings were derived from the data-driven approach. Here, 10 nodes showing the highest centrality values in both HCA and ACA individuals (bilateral putamen, bilateral precuneus, bilateral superior frontal, bilateral insula, left superior parietal, and right thalamus) were removed from the network. Most of these nodes belong to the Rich Club network comprising structural hubs in the cerebral cortex, central in

communication and integration across the brain, as well as relevant for varied cognitive functions (van Den Heuvel & Sporns, 2013).

Before recovering the findings derived from this data-driven approach, it must be underscored that the most and least connected nodes were similarly rank-ordered in HCA and ACA individuals. The betweenness values computed for the 82 nodes in the HCA individuals were highly correlated with the values computed for ACA individuals (Speaman rank-order correlation, r_s = 0.94). Importantly, the same correlational pattern emerges for ACA individuals recruited from the HCP and the ACA individuals scanned with exactly the same MRI machine than the HCA individuals. The r_s values were: ACA-HCP x ACA-Madrid = 0.86 and ACA-Madrid x HCA = 0.84. Therefore, the potential site effect must be meager, if present at all.

The finding that the most and least connected nodes in the brain structural network are shared by all individuals, regardless of their general cognitive status, is not coherent with the functional findings reported by (Santarnecchi et al., 2015). Their results suggest that individuals with higher and lower general cognitive ability could be characterized by distinguishable functional networks (language and memory processing networks versus emotional processing networks, respectively). However, the result observed here implies that the greater brain resilience of HCA individuals is merely quantitative: the structural brain network they share with ACA individuals is stronger, but not qualitatively different. The results reported here revealed that HCA individuals keep their network stability, as assessed by global and local efficiency values, when the most central nodes are removed, whereas these values worsened in ACA individuals. Therefore, like the findings observed in the theory-driven approach, the brain structural connectomes of HCA individuals seem

capable to overcome the attacks applied to Rich Club central hubs by means of some sort of network adaptive reconfiguration.

4.2. Why are the structural brain networks of HCA individuals more resilient?

This is a key question still requiring sound answers. One that could be generalizable beyond the cognitive domain might be an interesting choice. In this regard, Caspi and Moffitt (2018) discussed at length the system integrity framework for explaining the observed generalized vulnerability to psychopathology (represented by the so-called **p** factor). One of the hypotheses addressed by these authors relates to deficits in general cognitive ability (GCA). It has been documented that adult individuals showing higher levels of **p** are characterized by low cognitive performance in measures of attention control, visual-perceptual processing and visual-motor coordination already in their childhood, before the onset of their mental disorders. This is also related to the concept of cognitive reserve (Ruíz Sánchez De León, Quiroga, & Colom, 2019). Low levels of general cognitive ability in childhood are associated with future higher **p** levels probably because the former "is a marker of neuroanatomical deficits that increase the vulnerability to multiple different common psychiatric disorders". The brain is behind both, cognitive ability and mental disorders, and, therefore, it is reasonable to connect these dots. McTeague et al. (2017) found, in this regard, that problems of cognitive control are shared by varied mental disorders (schizophrenia, bipolar disorder, OCD, depression, anxiety, and addiction) also sharing brain networks including the cingulate cortex and the anterior insulae.

From a cognitive epidemiology perspective, Calvin et al. (2017) discussed the integrity hypothesis for explaining why cognitive ability measured in childhood (age 11) is

inversely associated with major causes of death (respiratory disease, coronary heart disease, stroke, injury, smoking related cancers, digestive disease, and dementia are some examples) six decades later (age 79). The short story is that cognitive ability and disease biomarkers may tap a latent trait of optimal bodily function (Arden et al., 2016; Davies et al., 2018; Deary, 2012; Hill, Harris, & Deary, 2019). The long story may unfold using the work by (Karama et al., 2014). These authors analyzed 588 individuals from the Lothian Birth Cohort 1936, obtaining cognitive ability measures at age 11 and at age 70, along with structural MRI data at age 73. The key finding revealed that more than two thirds of the association between cognitive ability measured at age 70 with cortical thickness measured at age 73 was explained by cognitive ability measured at age 11. Three potential explanations for this finding were offered: (1) genetic factors contributing to cognitive ability differences in childhood are also relevant in old age, as well as for brain growth and maintenance; (2) individuals with higher cognitive ability are more physically and mentally active than individuals with lower cognitive ability; and (3) reciprocal associations between cognitive and brain development. The first explanation is closely related with the integrity hypothesis discussed above, whereas this is not the case for the second and third explanations. The cross-lagged study by Estrada, Ferrer, Roman, Karama, and Colom (2019) did provide results consistent with the third explanation: the magnitude (rate) of longitudinal changes in cognitive and cortical development across time (but not previous levels on any of these variables) did predict later changes in both cognition and brain features such as cortical thickness and cortical surface area.

4.3. Resilience and stimulation

There are two related issues that deserve discussion. First, the greater resilience of HCA individuals may be related with findings observed in brain stimulation studies. Santarnecchi and Rossi (2016) discussed evidence showing that individuals with lower cognitive ability obtain greater benefit from brain stimulation, whereas individuals with higher cognitive ability are less responsive to it because their cognitive system may be "already optimized for the task at hand and, therefore, shielded against perturbation". Secondly, these findings derived from brain stimulation studies are remarkably consistent with results observed in cognitive training studies using a neuroimaging approach. As summarized by Colom and Román (2018): (a) brain structural features such as cortical thickness and cortical surface area, are more sensitive to cognitive interventions in individuals with lower cognitive ability (Román et al., 2016) and (b) brain structural networks are also sensitive to these cognitive interventions (Román et al., 2017).

These facts open the door to the possibility of finding ways to increase the resilience of the brain networks in ACA individuals by mimicking those identified in HCA individuals. This resembles the cognitive epidemiology approach: "what seems more likely to be effective is to encourage phenocopies of high intelligence with respect to health. Formally, a phenocopy means an individual whose environmentally produced phenotypic characteristics is the same as that normally produced by a gene; here, we use it to mean people's copying what people of higher intelligence do with respect to health behaviors. To the extent that researchers can discover what smart people do to look after their bodies and health and manage their illnesses, these strategies can be made widely known and available as valid and useful health-care rules" (Deary, Weiss, & Batty, 2010).

If structural networks can change as a result of targeted psychological interventions (Colom & Roman, 2018), we may think in designing efficient (personalized) procedures for achieving a greater distributed processing capacity in ACA individuals and, especially, in those showing low cognitive ability levels. Research suggests that individuals with low cognitive ability levels benefit most from psychological and educational interventions (Hegelund et al., 2020), and, therefore, the promise of increasing the distributed processing capacity of their brains stimulating their connectomes may not be just science-fiction (Clark et al., 2012; Cohen Kadosh, Soskic, Iuculano, Kanai, & Walsh, 2010; Haier, 2017; Keizer, Verschoor, Verment, & Hommel, 2010; Santarnecchi et al., 2013).

4.4. Limitations

All research studies can be characterized by strengths and weaknesses. Methodological details can always be improved and movements forward in this regard contribute to obtain increased valuable knowledge, albeit always open to further scrutiny. We can identify two main weaknesses or limitations in the present study.

Firstly, the distribution of streamlines among regions is linked to the integrity of the connections in the structural network. This is presumably related to white matter physiology, because those streamlines are calculated by measuring the diffusion behavior of water molecules in white matter fibers. Therefore, it can be inferred that the observed trends of the network integrity indices considered here, GE and LE, are linked to white matter physiology network properties. Nevertheless, the behavior of a mathematical network of 82 regions comprised of probabilistically generated streamlines is vastly different from the anatomical microscopic network formed by the actual white matter

fibers themselves. The different characteristics measured by GE and LE relate to the different processing capabilities of the network (global versus local), and given that the networks are being disrupted with violent attacks, both by TAs and RAs, it is no surprise that these indices behave similarly. Having a much more fine-grained atlas that could comprise smaller regions than the 82 used in the present study might show some more differences in the global and local processing methods of each network.

Secondly, the disparate findings based on the quantitative (structural) versus qualitative (functional) network differences, raises the requirement of analyzing the same individuals using both types of data. The question of why brain resilience manifests in such different ways analyzing structural and functional evidence deserves further close attention.

4.5. Conclusion

In conclusion, here we have shown that individuals with very high general cognitive ability are more resilient to targeted attacks directed at their structural brain network than individuals with average general cognitive ability. However, although the mean cognitive difference was greater than two standard deviations, the largest mean difference at the brain level was around one standard deviation. The difference between both values strongly suggests that there are further variables involved. At the brain level, structure does not tell the whole story, and, therefore, functional evidence should be obtained and integrated to obtain a wider picture. The social network is also undoubtedly involved. Cognitive ability and the related brain features do interact with environmental variables. Obtaining a big picture requires integrating the different pieces of the puzzle. Finally, we can point to a thought-provoking issue raised by Karpinski, Kinase Kolb, Tetreault and Borowski (2018), that we believe deserves attention: is there

a relationship between heightened cognitive ability and increased negative bodily signs? Highly intelligent individuals may show significantly greater risk for disorders at the end of the day. Their research found some supporting evidence regarding health, but data at the brain level are strongly required.

5. REFERENCES

Alstott, J., Breakspear, M., Hagmann, P., Cammoun, L., & Sporns, O. (2009). Modeling the impact of lesions in the human brain (modeling lesions in human brain). *PLoS Computational Biology, 5*(6), e1000408. doi:10.1371/journal.pcbi.1000408

Arden, R., Luciano, M., Deary, I. J., Reynolds, C. A., Pedersen, N. L., Plassman, B. L., . . . Visscher, P. M. (2016). The association between intelligence and lifespan is mostly genetic. *International Journal of Epidemiology, 45*(1), 178-185. doi:10.1093/ije/dyv112

Barbey, A. K., Karama, S., & Haier, R. J. (2021). In Barbey A. K., Karama S. and Haier R. J. (Eds.), *The Cambridge Handbook of Intelligence and Cognitive Neuroscience* Cambridge University Press (In Press).

Barbey, A. K., Colom, R., Solomon, J., Krueger, F., Forbes, C., & Grafman, J. (2012). An integrative architecture for general intelligence and executive function revealed by lesion mapping. *Brain: A Journal of Neurology, 135*, 1154-1164. doi:10.1093/brain/aws021

Barbey, A., Colom, R., Paul, E., & Grafman, J. (2014). Architecture of fluid intelligence and working memory revealed by lesion mapping. *Brain Structure and Function, 219*(2), 485-494. doi:10.1007/s00429-013-0512-z

Basten, U., Hilger, K., & Fiebach, C. (2015). Where smart brains are different: A quantitative meta-analysis of functional and structural brain imaging studies on intelligence. *Intelligence, 51*, 10.

Bilker, W. B., Hansen, J. A., Brensinger, C. M., Richard, J., Gur, R. E., & Gur, R. C. (2012). Development of abbreviated nine-item forms of the raven's standard progressive matrices test. *Assessment, 19*(3), 354-369. doi:10.1177/1073191112446655

Calvin, C. M., Batty, G. D., Der, G., Brett, C. E., Taylor, A., Pattie, A., . . . Deary, I. J. (2017). *Childhood intelligence in relation to major causes of death in 68 year follow-up: Prospective population study* British Medical Journal Publishing Group. doi:10.1136/bmj.j2708

Caspi, A., & Moffitt, T. E. (2018). All for one and one for all: Mental disorders in one dimension. *The American Journal of Psychiatry, 175*(9), 831-844. doi:10.1176/appi.ajp.2018.17121383 [doi]

Clark, V. P., Coffman, B. A., Mayer, A. R., Weisend, M. P., Lane, T. D. R., Calhoun, V. D., . . . Wassermann, E. M. (2012). TDCS guided using fMRI significantly accelerates learning to identify concealed objects. *NeuroImage, 59*(1), 117-128. doi:10.1016/j.neuroimage.2010.11.036

Cohen Kadosh, R., Soskic, S., Iuculano, T., Kanai, R., & Walsh, V. (2010). Modulating neuronal activity produces specific and long-lasting changes in numerical competence. *Current Biology, 20*(22), 2016-2020. doi:10.1016/j.cub.2010.10.007

Colom, R. (2014). From the earth to the brain. *Personality and Individual Differences, 61-62*, 3-6. doi:10.1016/j.paid.2013.12.025

Colom, R., Burgaleta, M., Román, F.,J., Karama, S., Álvarez-Linera, J., Abad, F. J., . . . Haier, R. J. (2013). Neuroanatomic overlap between intelligence and cognitive factors: Morphometry methods provide support for the key role of the frontal lobes. *NeuroImage, 72*, 143-152. doi:10.1016/j.neuroimage.2013.01.032

Colom, R., Karama, S., Jung, R. E., & Haier, R. J. (2010). Human intelligence and brain networks. *Dialogues in Clinical Neuroscience, 12*(4), 489-501. Retrieved from https://pubmed.ncbi.nlm.nih.gov/21319494; https://www.ncbi.nlm.nih.gov/pmc/articles/PMC3181994/

Colom, R., & Román, F. J. (2018). Enhancing intelligence: From the group to the individual. *Journal of Intelligence, 6*(1), 11. doi:10.3390/jintelligence6010011

Colom, R., & Thompson, P. M. (2011). Understanding human intelligence by imaging the brain. *The Wiley-Blackwell Handbook of Individual Differences.* (pp. 330-352) Wiley-Blackwell.

Davies, G., Lam, M., Harris, S. E., Trampush, J. W., Luciano, M., Hill, W. D., ... (2018). Study of 300,486 individuals identifies 148 independent genetic loci influencing general cognitive function.*9*(1) doi:10.1038/s41467-018-04362-x

Deary, I. J. (2012). Looking for 'system integrity' in cognitive epidemiology. *Gerontology, 58*(6), 545-553. doi:10.1159/000341157 [doi]

Deary, I. J., Weiss, A., & Batty, G. D. (2010). Intelligence and personality as predictors of illness and death: How researchers in differential psychology and chronic disease

epidemiology are collaborating to understand and address health inequalities. *Psychological Science in the Public Interest, 11*(2), 53-79. doi:10.1177/1529100610387081

Desikan, R. S., Ségonne, F., Fischl, B., Quinn, B. T., Dickerson, B. C., Blacker, D., . . . Killiany, R. J. (2006). An automated labeling system for subdividing the human cerebral cortex on MRI scans into gyral based regions of interest. *NeuroImage, 31*(3), 968-980. doi:10.1016/j.neuroimage.2006.01.021

Dubois, J., Galdi, P., Paul, L. K., & Adolphs, R. (2018). A distributed brain network predicts general intelligence from resting-state human neuroimaging data. *Philosophical transactions of the Royal Society of London. Series B, Biological sciences*, *373*(1756), 20170284. https://doi.org/10.1098/rstb.2017.0284

Ebisch, S. J., Perrucci, M. G., Mercuri, P., Romanelli, R., Mantini, D., Romani, G. L., . . . Saggino, A. (2012). Common and unique neuro-functional basis of induction, visualization, and spatial relationships as cognitive components of fluid intelligence. *NeuroImage, 62*(1), 331-342. doi:10.1016/j.neuroimage.2012.04.053

Escorial, S., Román, F.,J., Martínez, K., Burgaleta, M., Karama, S., & Colom, R. (2015). Sex differences in neocortical structure and cognitive performance: A surface-based morphometry study. *NeuroImage, 104*, 355-365. doi:10.1016/j.neuroimage.2014.09.035

Estrada, E., Ferrer, E., Roman, F. J., Karama, S., & Colom, R. (2019). Time-lagged associations between cognitive and cortical development from childhood to early adulthood. *Developmental Psychology, 55*(6), 1338-1352. doi:10.1037/dev0000716 [doi]

Euler, M. J. (2018). Intelligence and uncertainty: Implications of hierarchical predictive processing for the neuroscience of cognitive ability. *Neuroscience and Biobehavioral Reviews, 94*, 93-112. doi:10.1016/j.neubiorev.2018.08.013

Fischl, B., van der Kouwe, A., Destrieux, C., Halgren, E., Segonne, F., Salat, D. H., . . . Dale, A. M. (2004). Automatically parcellating the human cerebral cortex. *Cerebral Cortex (New York, N.Y.: 1991), 14*(1), 11-22. doi:10.1093/cercor/bhg087 [doi]

Funder, D. C., & Ozer, D. J. (2019). Evaluating effect size in psychological research: Sense and nonsense. *Advances in Methods and Practices in Psychological Science, 2*(2), 156-168. doi:10.1177/2515245919847202

Gignac, G. E., & Bates, T. C. (2017). Brain volume and intelligence: The moderating role of intelligence measurement quality. *Intelligence, 64*, 18-29. doi:10.1016/j.intell.2017.06.004

Gläscher, J., Tranel, D., Paul, L. K., Rudrauf, D., Rorden, C., Hornaday, A., . . . Adolphs, R. (2009). Lesion mapping of cognitive abilities linked to intelligence. *Neuron, 61*(5), 681-691. doi:10.1016/j.neuron.2009.01.026

Gläscher, J., Rudrauf, D., Colom, R., Paul, L. K., Tranel, D., Damasio, H., & Adolphs, R. (2010). Distributed neural system for general intelligence revealed by lesion mapping. *Proceedings of the National Academy of Sciences of the United States of America*, *107*(10), 4705–4709. https://doi.org/10.1073/pnas.0910397107

Haier, R. J. (2017). *The neuroscience of intelligence* Cambridge University Press.

Hegelund, E. R., Grønkjær, M., Osler, M., Dammeyer, J., Flensborg-Madsen, T., & Mortensen, E. L. (2020). The influence of educational attainment on intelligence. *Intelligence, 78* doi:10.1016/j.intell.2019.101419

Hill, W. D., Harris, S. E., & Deary, I. J. (2019). What genome-wide association studies reveal about the association between intelligence and mental health. *Current Opinion in Psychology, 27*, 25-30. doi:10.1016/j.copsyc.2018.07.007

Jung, R. E., & Haier, R. J. (2007). The parieto-frontal integration theory (P-FIT) of intelligence: Converging neuroimaging evidence. *Behavioral and Brain Sciences, 30*(2), 135-154. doi:10.1017/S0140525X07001185

Karama, S., Bastin, M. E., Murray, C., Royle, N. A., Penke, L., Munoz Maniega, S., . . . Deary, I. J. (2014). Childhood cognitive ability accounts for associations between cognitive ability and brain cortical thickness in old age. *Molecular Psychiatry, 19*(5), 555-559. doi:10.1038/mp.2013.64 [doi]

Karama, S., Colom, R., Johnson, W., Deary, I. J., Haier, R., Waber, D. P., . . . Evans, A. C. (2011). Cortical thickness correlates of specific cognitive performance accounted for by the general factor of intelligence in healthy children aged 6 to 18. *NeuroImage, 55*(4), 1443-1453. doi:10.1016/j.neuroimage.2011.01.016

Karpinski, R. I., Kinase Kolb, A.,M., Tetreault, N. A., & Borowski, T. B. (2018). High intelligence: A risk factor for psychological and physiological overexcitabilities. *Intelligence* (Norwood), 66, 8-23. doi:10.1016/j.intell.2017.09.001

Keizer, A. W., Verschoor, M., Verment, R. S., & Hommel, B. (2010). The effect of gamma enhancing neurofeedback on the control of feature bindings and

intelligence measures. *International Journal of Psychophysiology, 75*(1), 25-32. doi:10.1016/j.ijpsycho.2009.10.011

Martínez, K., & Colom, R. (2021). Imaging the intelligence of humans. In A. K. Barbey, S. Karama & R. J. Haier (Eds.), *The Cambridge Handbook of Intelligence and Cognitive Neuroscience*. Cambridge University Press (In Press).

Martínez, K., Madsen, S. K., Joshi, A. A., Joshi, S. H., Román, F. J., Villalon-Reina, J., . . . Colom, R. (2015). Reproducibility of brain-cognition relationships using three cortical surface-based protocols: An exhaustive analysis based on cortical thickness. *Human Brain Mapping, 36*(8), 3227-3245. doi:10.1002/hbm.22843

McTeague, L. M., Huemer, J., Carreon, D. M., Jiang, Y., Eickhoff, S. B., & Etkin, A. (2017). Identification of common neural circuit disruptions in cognitive control across psychiatric disorders. *The American Journal of Psychiatry, 174*(7), 676-685. doi:10.1176/appi.ajp.2017.16040400 [doi]

Moore, T. M., Reise, S. P., Gur, R. E., Hakonarson, H., & Gur, R. C. (2015). Psychometric properties of the Penn Computerized Neurocognitive Battery. *Neuropsychology*, *29*(2), 235–246. https://doi.org/10.1037/neu0000093

Pineda-Pardo, J., Martínez, K., Román, F.,J., & Colom, R. (2016). Structural efficiency within a parieto-frontal network and cognitive differences. *Intelligence, 54*, 105-116. doi:10.1016/j.intell.2015.12.002

Román, F. J., Abad, F. J., Escorial, S., Burgaleta, M., Martínez, K., Álvarez-Linera, J., . . . Colom, R. (2014). Reversed hierarchy in the brain for general and specific

cognitive abilities: A morphometric analysis. *Human Brain Mapping, 35*(8), 3805-3818. doi:10.1002/hbm.22438

Román, F. J., Lewis, L., Chen, C., Karama, S., Burgaleta, M., Martínez, K., . . . Colom, R. (2016). Gray matter responsiveness to adaptive working memory training: A surface-based morphometry study. *Brain Structure and Function, 221*(9), 4369-4382. doi:10.1007/s00429-015-1168-7

Román, F.,J., Iturria-Medina, Y., Martínez, K., Karama, S., Burgaleta, M., Evans, A. C., . . . Colom, R. (2017). Enhanced structural connectivity within a brain sub-network supporting working memory and engagement processes after cognitive training. *Neurobiology of Learning and Memory, 141*, 33-43. doi:10.1016/j.nlm.2017.03.010

Ruíz Sánchez De León, J. M., Quiroga, M. Á, & Colom, R. (2019). Intelligence and executive function: Can we reunite these disparate worlds? In D. J. McFarland (Ed.), *General and specific mental abilities* (pp. 311-339) Cambridge Scholars Publisher.

Santarnecchi, E., & Rossi, S. (2016). Advances in the neuroscience of intelligence: From brain connectivity to brain perturbation. *The Spanish Journal of Psychology, 19*, E94. doi:S1138741616000895 [pii]

Santarnecchi, E., Galli, G., Polizzotto, N. R., Rossi, A., & Rossi, S. (2014). Efficiency of weak brain connections support general cognitive functioning. *Human Brain Mapping, 35*(9), 4566-4582. doi:10.1002/hbm.22495

Santarnecchi, E., Polizzotto, N. r., Godone, M., Giovannelli, F., Feurra, M., Matzen, L., . . . Rossi, S. (2013). Frequency-dependent enhancement of fluid intelligence induced

by transcranial oscillatory potentials. *Current Biology, 23*(15), 1449-1453. doi:10.1016/j.cub.2013.06.022

Santarnecchi, E., Rossi, S., & Rossi, A. (2015). The smarter, the stronger: Intelligence level correlates with brain resilience to systematic insults. *Cortex, 64*, 293-309. doi:10.1016/j.cortex.2014.11.005

Smith, R. E., Tournier, J. D., Calamante, F., & Connelly, A. (2013). SIFT: Spherical-deconvolution informed filtering of tractograms. *NeuroImage, 67*, 298-312. doi:10.1016/j.neuroimage.2012.11.049 [doi]

Sporns, O., & Zwi, J. D. (2004). The small world of the cerebral cortex. *Neuroinformatics, 2*(2), 145-162. doi:NI:2:2:145 [pii]

Sternberg, R. J. (2020). *The Cambridge Handbook of Intelligence.* Cambridge University Press.

Vaidya, A. R., Pujara, M. S., Petrides, M., Murray, E. A., & Fellows, L. K. (2019). Lesion studies in contemporary neuroscience. *Trends in Cognitive Sciences, 23*(8), 653-671. doi:10.1016/j.tics.2019.05.009

Vakhtin, A. A., Ryman, S. G., Flores, R. A., & Jung, R. E. (2014). Functional brain networks contributing to the parieto-frontal integration theory of intelligence. *NeuroImage, 103*, 349-354. doi:10.1016/j.neuroimage.2014.09.055

van Den Heuvel, M.,P., & Sporns, O. (2013). Network hubs in the human brain. *Trends in Cognitive Sciences, 17*(12), 683-696. doi:10.1016/j.tics.2013.09.012

Williams, J. E., & McCord, D. M. (2006). *Equivalence of standard and computerized versions of the raven progressive matrices test* doi:https://doi.org/10.1016/j.chb.2004.03.005

FIGURE LEGENDS

Figure 1. Distribution of PMAT-24 scores for the ACA (Average Cognitive Ability, Mean = 15.05, SD = 3.99) and HCA (High Cognitive Ability, Mean = 22.60, SD = 1.35) individuals.

Figure 2. (a) Workflow for connectivity matrix generation, **(b)** graph metrics computation, **(c)** centrality-based ranking of nodes, and **(d)** targeted and randomized attacks to the structural brain network. For visualization purposes, the SIFT filtered 1 million streamlines tractogram image in (a) has been reduced to a 200,000 streamlines image.

Figure 3. Network integrity indices after applying targeted attacks (TAs). In the **left panel**, individual values of network integrity properties are plotted against the nodes removed for each network in HCA and ACA individuals. In the **right panel**, the change in value of the property (defined as the original value without any perturbance minus the value right before the network collapses) is plotted against the individual value in the PMAT-24 score.

Figure 4. Network integrity indices after randomized attacks (RAs). In the **left panel**, individual values of network integrity properties are plotted against the nodes removed for each network in HCA and ACA individuals. In the **right panel**, the change in value of the property (defined as the original value without any perturbance minus the value

right before the network collapses) is plotted against the individual value on the PMAT-24 score.

Figure 5. (a) Parieto-Frontal Theory Nodes. Colored nodes represent regions included in the stages 2 and 4 proposed in the model. **(b)** Network integrity indices (GE and LE) for HCA and ACA individuals before nodes removal and after removing nodes comprised by stages 2 (information integration) and 4 (response selection) of the P-FIT model. SMG: supramarginal gyrus; PCU: precuneus; SPG: superior parietal gyrus; ACG: anterior cingulate gyrus. R: right hemisphere; L: left hemisphere.

Figure 6. (a) Top 12 nodes in the structural networks. Colors highlight most central (highest betweenness) nodes for HCA (red), ACA (blue) and those shared by both cognitive ability groups (violet). **(b)** Network integrity indices (GE and LE) for HCA and ACA individuals before nodes removal and after removing their most important shared nodes (violet nodes in a.). SFG: superior frontal gyrus, PU = putamen, INS: insula; TH: thalamus; ICG: inferior cingulate gyrus; PCU: precuneus; SPG: superior parietal gyrus; L: left hemisphere.

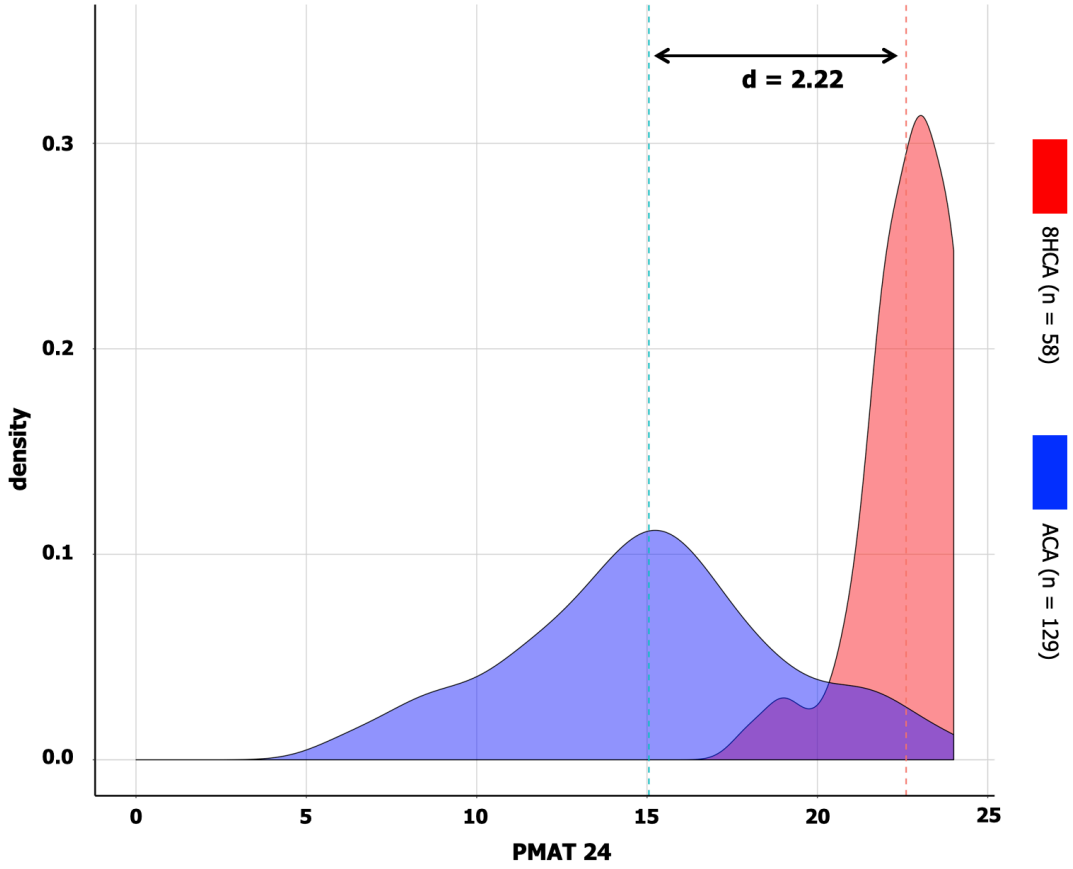

FIGURE 1

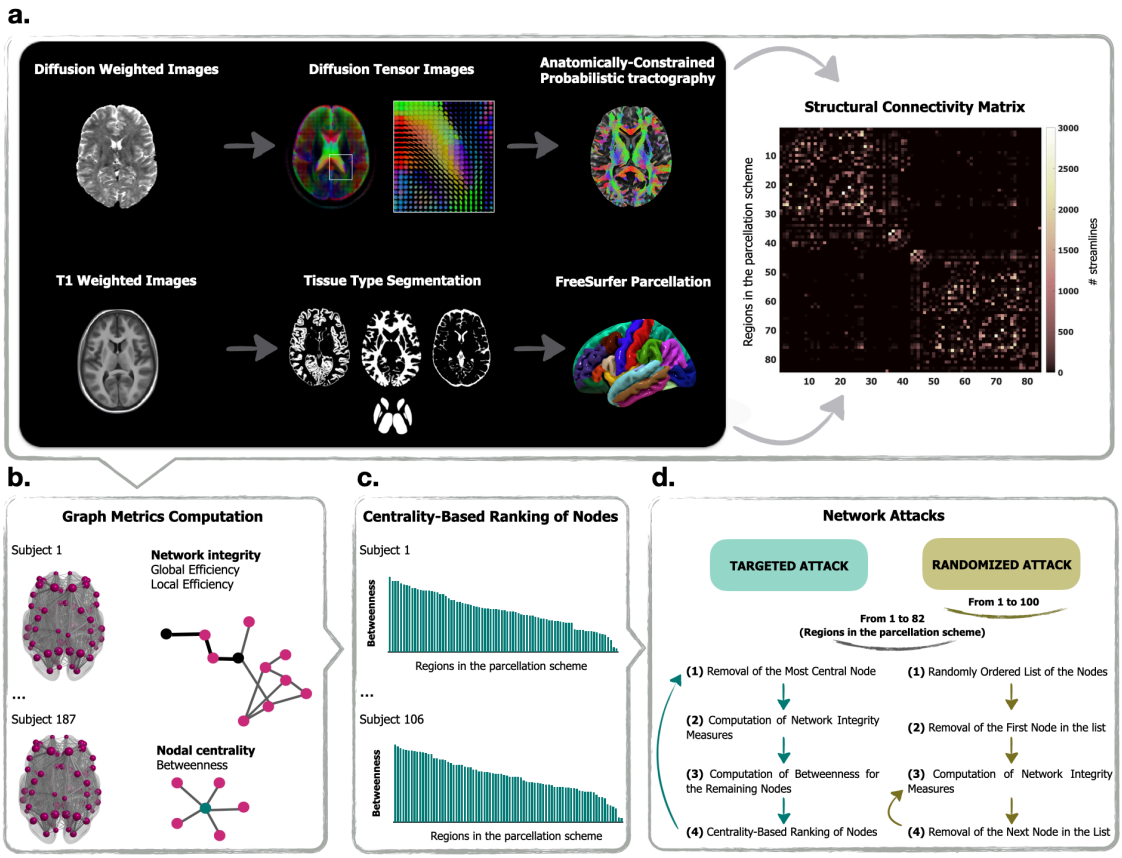
a.
Diffusion Weighted Images
Diffusion Tensor Images
Anatomically-Constrained Probabilistic tractography
T1 Weighted Images
Tissue Type Segmentation
FreeSurfer Parcellation
Structural Connectivity Matrix
Regions in the parcellation scheme
streamlines
b.
Graph Metrics Computation
Subject 1
Network integrity
Global Efficiency
Local Efficiency
Subject 187
Nodal centrality
Betweenness
c.
Centrality-Based Ranking of Nodes
Subject 1
Betweenness
Regions in the parcellation scheme
Subject 106
d.
Network Attacks
TARGETED ATTACK
RANDOMIZED ATTACK
From 1 to 100
From 1 to 82
(Regions in the parcellation scheme)
(1) Removal of the Most Central Node
(2) Computation of Network Integrity Measures
(3) Computation of Betweenness for the Remaining Nodes
(4) Centrality-Based Ranking of Nodes
(1) Randomly Ordered List of the Nodes
(2) Removal of the First Node in the list
(3) Computation of Network Integrity Measures
(4) Removal of the Next Node in the List

FIGURE 2

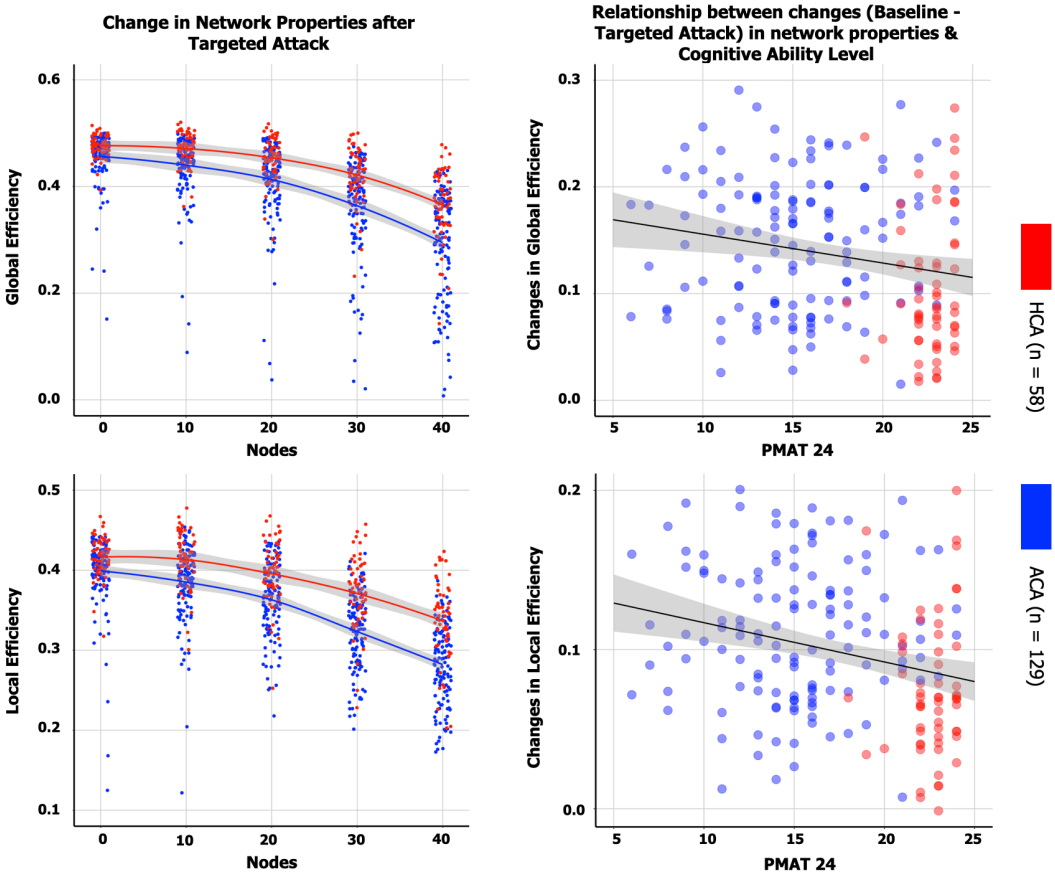
Change in Network Properties after Targeted Attack
Global Efficiency
Nodes
Local Efficiency
Nodes
Relationship between changes (Baseline - Targeted Attack) in network properties & Cognitive Ability Level
Changes in Global Efficiency
PMAT 24
Changes in Local Efficiency
PMAT 24
HCA (n = 58)
ACA (n = 129)

FIGURE 3

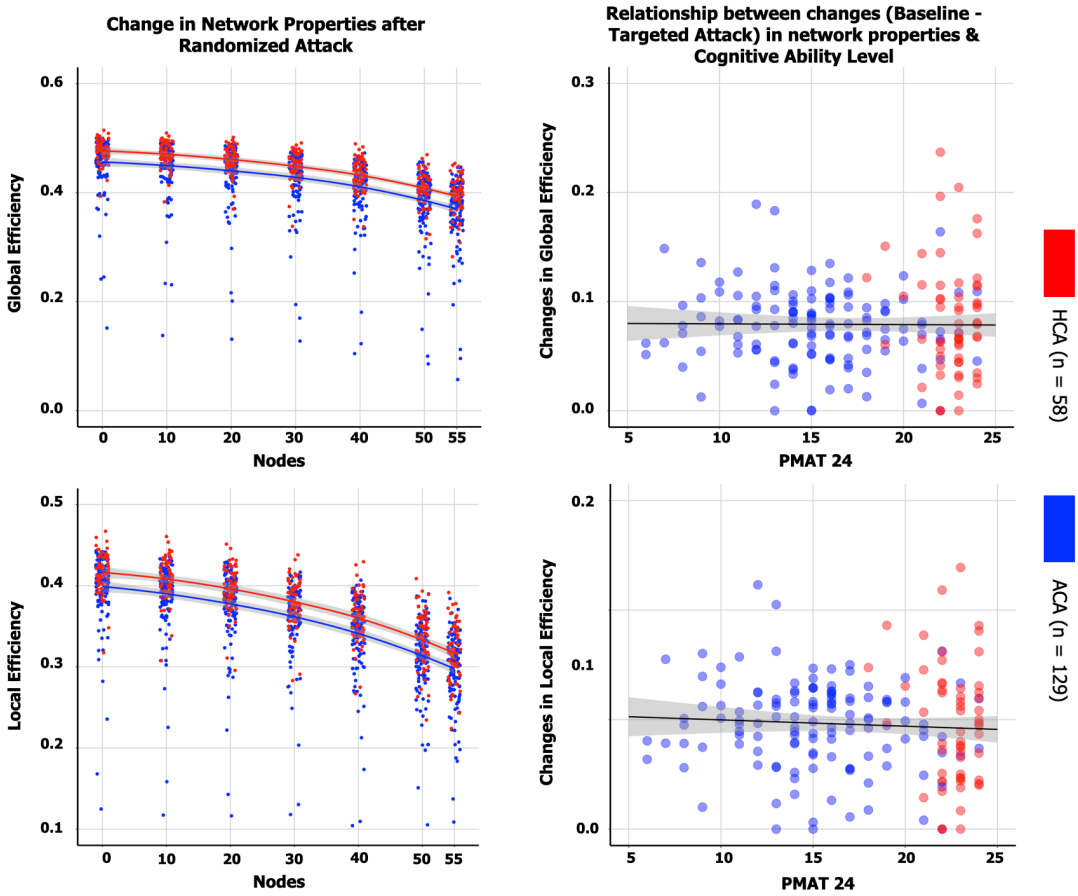
Change in Network Properties after Randomized Attack
Global Efficiency
Nodes
Local Efficiency
Nodes
Relationship between changes (Baseline - Targeted Attack) in network properties & Cognitive Ability Level
Changes in Global Efficiency
PMAT 24
Changes in Local Efficiency
PMAT 24
HCA (n = 58)
ACA (n = 129)

FIGURE 4

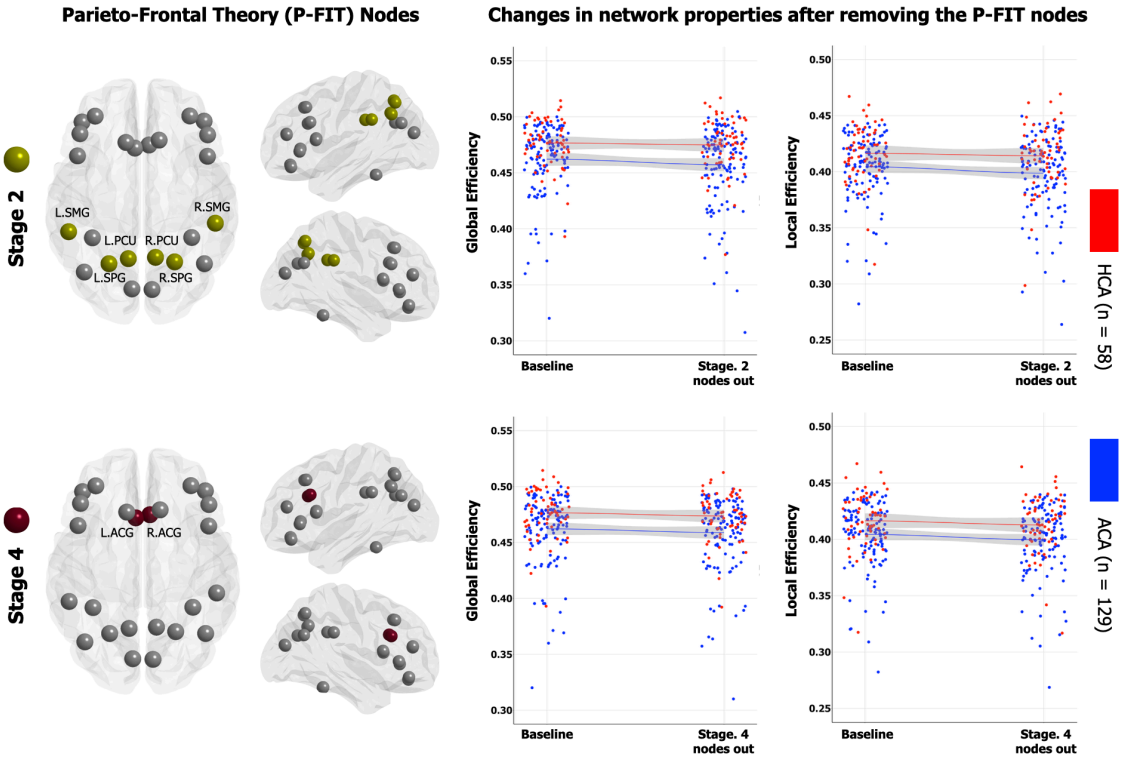
Parieto-Frontal Theory (P-FIT) Nodes
Changes in network properties after removing the P-FIT nodes
Stage 2
L.SMG
R.SMG
L.PCU
R.PCU
L.SPG
R.SPG
Stage 4
L.ACG
R.ACG
Global Efficiency
Local Efficiency
Baseline
Stage. 2 nodes out
Stage. 4 nodes out
HCA (n = 58)
ACA (n = 129)

FIGURE 5

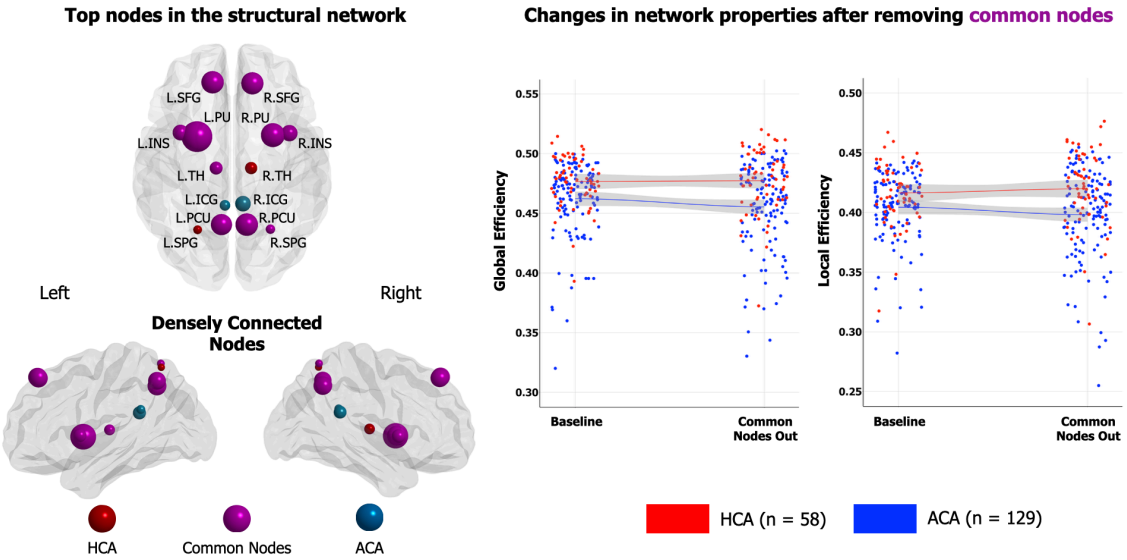
Top nodes in the structural network
L.SFG
R.SFG
L.PU
R.PU
L.INS
R.INS
L.TH
R.TH
L.ICG
R.ICG
L.PCU
R.PCU
L.SPG
R.SPG
Left
Right
Densely Connected Nodes
HCA
Common Nodes
ACA
Changes in network properties after removing common nodes
Global Efficiency
Local Efficiency
Baseline
Common Nodes Out
HCA (n = 58)
ACA (n = 129)

FIGURE 6

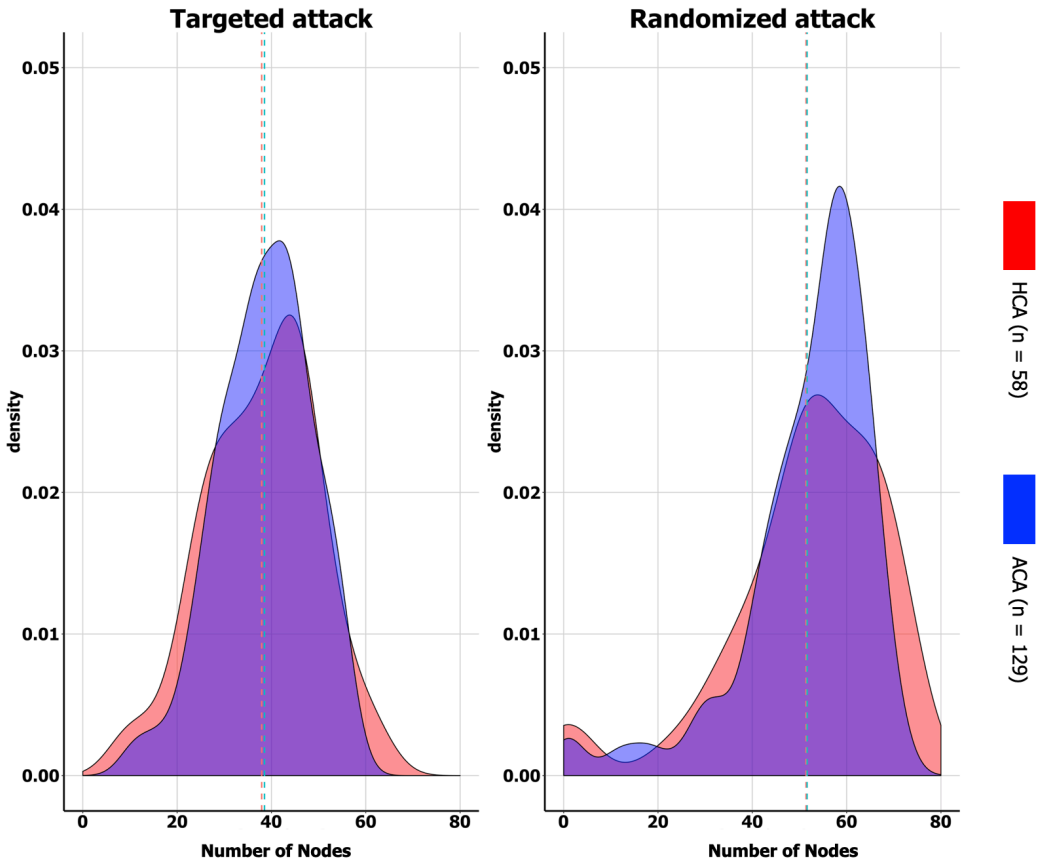

SUPPLEMENTARY FIGURE 1

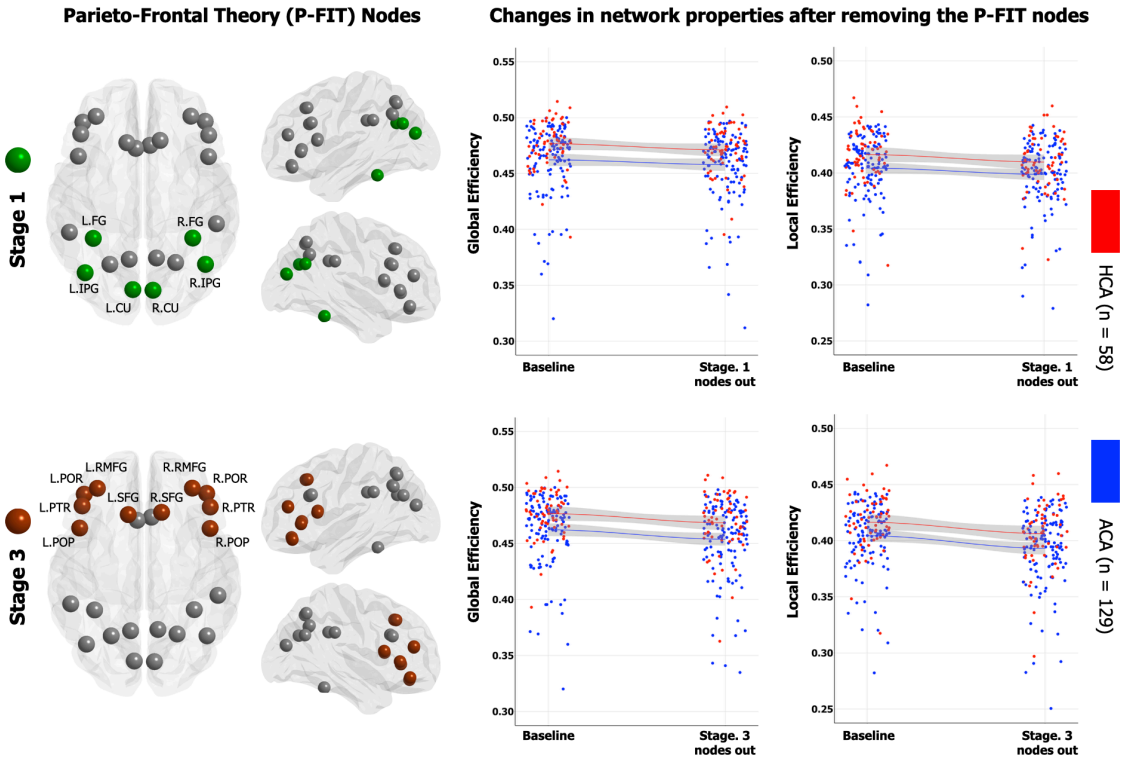

SUPPLEMENTARY FIGURE 2